Experimental Thermal and Fluid Science 136 (2022) 110662

Contents lists available at ScienceDirect

Experimental Thermal and Fluid Science

journal homepage: www.elsevier.com/locate/etfs

Comparison of characteristics evaluated by different fractal approaches of soot agglomerates produced by a combustion aerosol generator

Concepción Paz *, Adrián Cabarcos, Marcos Conde, Christian Gil

CINTECX, Universidade de Vigo, Campus Universitario Lagoas-Marcosende, Vigo 36310, Spain

ARTICLE INFO

Keywords:
Soot agglomerates
Soot generator
Thermophoretic sampling
TEM
Soot morphology
Fractal dimension

ABSTRACT

A study on the fractal geometry, morphology and mass properties of particulate matter carried away by the emissions of a combustion aerosol generation bench was performed. Individual soot agglomerates, collected from exhaust gases using a thermophoretic sampling device, were observed ex-situ using transmission electron microscopy. Those micrographs were firstly used to obtain projected areas, diameters of gyration, and primary particle diameters. Based on this information, the most common overlapping approaches used to estimate the number of primary particles were applied and compared. Morphological descriptors obtained from micrographs were also used to provide approximate estimates of fractal dimensions, mass and density values, as well as mobility and aerodynamic diameters for the agglomerates collected.

1. Introduction

It is well known that soot particles carried by combustion exhaust emissions contribute significantly to air pollution, causing a negative impact on both human health and the environment [1]. An increased mortality has been recently associated with soot particulate exposure, demonstrating clear relations between ultrafine particulate and elevated risk of serious diseases such as lung cancer or asthma [2–4].

The European community is familiar with this scientific framework. In fact, due to an increasingly restrictive legislation in terms of emissions allowed, a significant emission reduction has been achieved in the last decades for the main polluting sectors (i.e. transport, households, industry and agriculture) [5]. However, air quality targets put forward by European environmental directives remain a challenge [6,7]. For this reason, it is indispensable to increase the knowledge of combustion aerosols, in order to reduce particulate pollutants and to develop cleaner technologies.

In this sense, the study of the soot formation process has become an important research line over the last decades [8]. Those investigations have concluded that soot formation begins when fuel molecules are pyrolized into molecular precursors, which chemically grow until they form polycyclic aromatic hydrocarbons (PAHs) [9]. The evolution of those PAHs chains is not well understood nowadays but eventually, these molecules grow large enough to become soot nuclei during a nucleation step. Then, high temperatures typically involving flames promote soot nuclei to grow, giving rise to the formation of primary particles [10]. The experimental study of the primary particles has shown a solid and spherical shape for these structures [11]. Finally, their physical adherence involves the formation of the soot agglomerates [12,13], which are complex, irregular and curved structures connected through overlapping and/or carbon surface growth [14]. Soot agglomerates can be characterized as mass fractals, and their irregularity and morphological behavior can be quantified based on their fractal dimension [15]. Furthermore, it is also important to note that a fraction of the organic molecules formed as intermediate compounds due to this process may leave the flame in gas form. Those hydrocarbons, which were not transformed into ordered soot structures, can condense on the elemental particles forming an organic coating over the agglomerate [16].

It should also be pointed out that all those combustion-generated particulate emissions have been traditionally collected through filters [17]. However, the nanometric nature of the soot agglomerates has involved the development of specific methodologies to observe and analyze the particulate matter. In this sense, the thermophoretic sampling has become the most common intrusive technique used to collect soot agglomerates [18]. This technique is minimally invasive and requires no manipulation of the samples taken. In contrast, other intrusive procedures such as dilution or cooling present a significant risk of altering the original state of the nano-particulate, which could lead to significant measurement errors.

The thermophoretic sampling process, which was initially described

* Corresponding author.
E-mail address: cpaz@uvigo.es (C. Paz).

https://doi.org/10.1016/j.expthermflusci.2022.110662
Received 28 October 2021; Received in revised form 25 March 2022; Accepted 27 March 2022
Available online 29 March 2022

Nomenclature

A_p	Projected area of an agglomerate, nm
a	Projected area of a primary particle, nm
C	Cunningham slip correction factor, -
D	Diameter, nm
Dil_{air}	Dilution air, %
D_f	Fractal dimension, -
d_{pp}	Diameter of a primary particle, nm
FSN	Filter Smoke Number, -
K_f, K_α	Fractal prefactors, -
Kn	Knudsen number, -
m	Mass of soot agglomerates, fg
N	Number, -
N_2	Nitrogen of the oxidizing agent, %
R^2	Coefficient of determination, -
r_c, r_k	Position vectors, pixels
z'	Overlapping exponent, -

Greek

α	Overlapping factor, -
ρ	Density, g/cm^3
Đ¤	Equivalence ratio, -
χ	Shape factor, -

Subscripts

0	Standard condition.
a	Aerodynamic.
eff	Effective.
g	Gyration.
m	Mobility.
mix	Mixing flow.
pp	Primary particles.
px	Pixels.
ve	Volume equivalent.

by Dobbins and Megaridis [19], is based on a brief and controlled exposition of a cold surface into a hot flow. Due to this temperature gradient, there is a particle transport from the higher to the lower temperatures, which allows the deposition of soot agglomerates on the cold surface of a sample grid. Complementing thermophoretic sampling, transmission electron microscopy (TEM) has become a common method used to measure the geometrical properties of soot [20]. Several experimental studies can exemplify the successfully combined use of thermophoretic devices and TEM measurements [21,22]. In fact, TEM inspections are commonly used to directly analyze aggregate distributions, with the advantage of not requiring prior knowledge of the particle properties such as the size, density, or morphology. As main disadvantages, a careful inspection of the samples taken and subsequent analysis through an image processing software are usually required.

The use of direct reading instruments that measure mass, aerodynamic or mobility diameters are also widespread in soot particle characterization. The combined use of some of those devices allows complete descriptions of particulate matter. As examples of those kinds of facilities, McMurry et al. [23] described a tandem system composed of a differential mobility analyzer (DMA) and a particle mass analyzer, whereas Stein et al. [24] proposed an experimental setup based on a DMA and an aerodyne aerosol mass spectrometer. Those kinds of instruments are easily serviceable in laboratory test aerosols, but may not be readily available when monitoring exposures in workplaces [25]. In fact, some of those systems are still relatively new research tools currently only available to a limited number of laboratories [26]. Therefore, TEM analysis still involves a powerful and useful off-line method for the characterization of soot particulate. Notwithstanding microscopy samples of workplace aerosols are often reachable and can be used to characterize particle morphology, there is a lack of studies that attempt to perform complete characterizations — size and fractal descriptors, equivalent diameters, mass and effective densities — from information available from TEM. Information obtained by those micrographs is rarely used beyond the calculation of primary particle diameters and projected areas.

In recent years, in order to study the formation and evolution of soot particulate under strictly controlled conditions, the use of calibrated sources such as soot generators has also increased [17,27]. By the use of these kinds of devices, which allow the generation of particulate ensuring repeatable conditions, recent studies have analyzed the chemical and morphological characteristics of soot emissions [28,29]. However, detailed characterizations of particulate matter emitted by those kinds of facilities remain at an early stage [17].

The objective of this study was to provide a complete characterization (fractal and size descriptors, equivalent diameters, mass and effective densities) of soot agglomerates emitted by a combustion aerosol generator bench. Those properties were obtained from the physical information available from the TEM inspection of soot agglomerates collected through a thermophoretic device. Furthermore, in order to characterize the number of primary particles per agglomerate, five different approaches were applied and statistically compared. The details of the calculation approach are presented and discussed.

2. Materials and methods

2.1. Experimental setup

The particulate matter examined in this study was generated employing an experimental test bench, which was designed to generate soot particulate under controlled conditions, and that was presented in detail in previous studies.

[30,31]. Fig. 1 depicts the scheme of the test facilities.

A combustion aerosol standard (Mini-Cast 5203 Type C) burner was used to produce the soot particulate.

[32]. Propane (purity > 99.9%) was used as the gaseous fuel and air mixed with N_2 as the oxidizing agent. Fig. 2a shows a schematic of the particle generation process of the Mini-Cast burner. Oxidizing agent is supplied coaxially to the fuel stream, allowing the generation of flames of different heights [33]. Once a flame has been established, soot particles are generated through hydrocarbon pyrolysis owing to the heat provided by the oxidation reaction at the flame front [34]. Nevertheless, a sudden interruption of the combustion process due to a dry nitrogen quench flow stabilizes the soot particles generated. The dilution air flow allows the particulate concentration to be reduced to a lower level [35].

Once these particles leave the burner, the temperature of the gas stream ranges from 80 °C to 140 °C. This gaseous stream then accesses the heating zone composed of a ceramic furnace and a 4.5 kW heating cable. The use of these devices allows the stream temperature to increase through conduction and radiation until values like those expected for diesel engines [36]. Experimental facilities equipped with burners and characterized by studies of other authors usually have similar devices. E. g., thermodenuders and catalytic strippers are commonly used to remove volatile compounds.

[16,17,37]. However, unlike those previous studies, the current work also involves a thermophoretic sampling step. Therefore, a favorable temperature gradient is also required to perform a successful sampling process. A thermophoretic sampling system, as shown in Fig. 2b, was employed to collect the particulate matter. This device

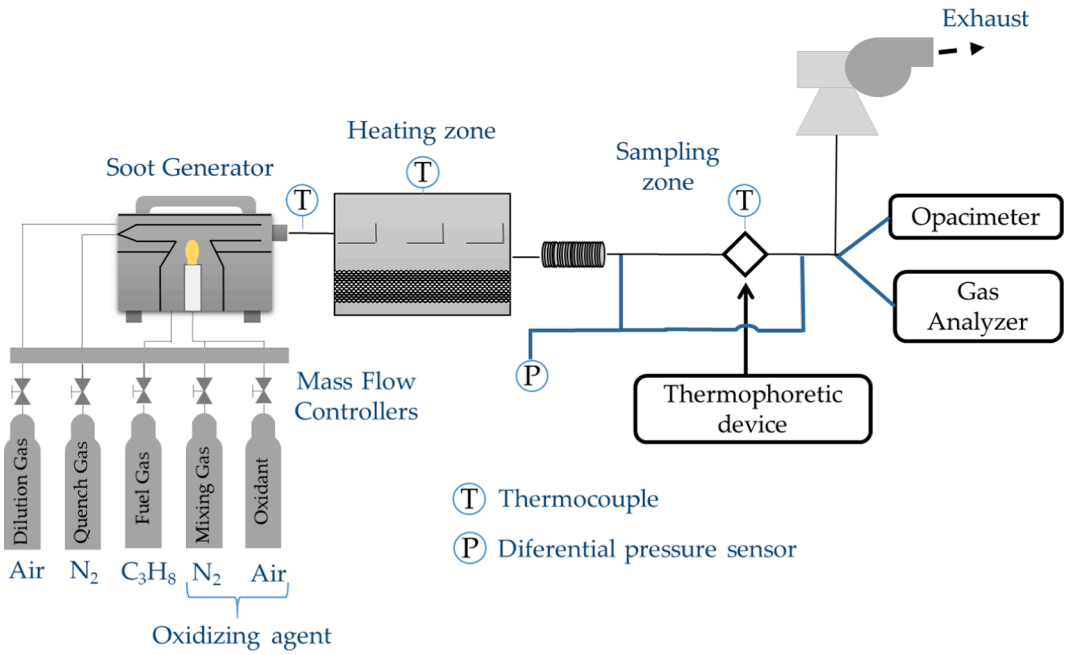

Fig. 1. Schematic of the test bench.

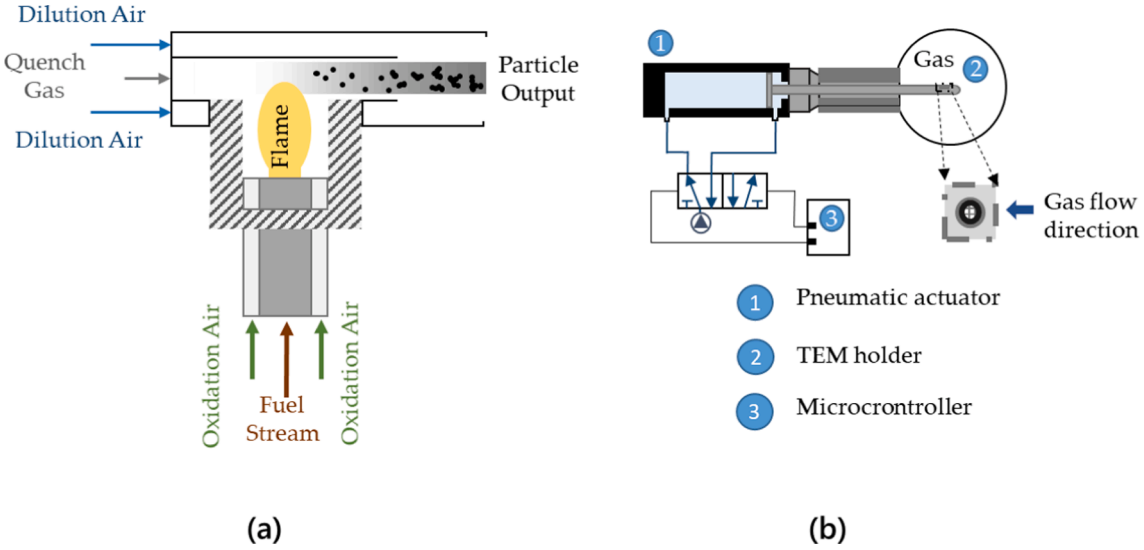

Fig. 2. **(a)** Soot generation process; (**b**) Thermophoretic sampling system.

consists of a pneumatic actuator that allows a fast insertion of the TEM holder inside the gas stream via a hole drilled in a vertical direction through the exhaust pipe [38]. Since the orientation of this system is crucial for a successful sampling, a poka-yoke guarantees a correct positioning of the device and, once the TEM holder is inside the hot flow field, the particulate matter is driven thermophoretically to the cold wall of the TEM sampling grid. In this study, 3 mm diameter 200 mesh PELCO® copper grids were specifically used to capture the agglomerates.

The measurement of the temperature is performed using various thermocouples (k-type, class-2 tolerance, ± 2.2 °C accuracy and 1.5 mm diameter). Measurements of the differential pressure upstream and downstream of the sampling zone are also carried out (Siemens Sitrans P500, 0.03% accuracy). All this information is recorded using an acquisition card NI USB-6363, which acquires the signal at a frequency of 1 kHz and filters it with a 2 Hz low-pass filter.

A DITEST GAS 1000 MDS 205 analyzer combined with a flame ionization detector (Horiba MEXA-1170HFID was used to determine the gas composition. Furthermore, an OPABOX opacimeter was used for measurements at the test bench exhaust outlet.

2.2. *Experimental procedure*

A total of seven test bench operating conditions were evaluated for this study. These settings —obtained varying gas flow rates and temperatures at the sampling zone — are shown in Table 1, where the equivalence ratio (Φ) is the relation between the fuel-to-oxidizer ratio to the stoichiometric one. The selection was based on the desire to produce aerosols of different concentrations and gas stream compositions. Those operating conditions were also chosen based on a previous work in order to produce emissions with high elemental carbon and thus obtain an onion-like graphitic refractory structure for primary particles [39]. Sampling temperatures were in the range of those values reported by Lapuerta et al. [38].

Table 1
Operating conditions of the test bench.

Operating condition	Quench gas (Nl/min)	Dilution (air) (Nl/min)	Oxidant (air) (Nl/min)	Mixing N_2 (Nl/min)	Equivalence ratio, Φ (-)	Sampling temperature (°C)
#1	10	100	4.2	0.0	1.13	221.17
#2	10	100	4.1	0.1	1.16	219.07
#3	10	100	3.9	0.3	1.22	221.71
#4	10	88.8	4.2	0.0	1.13	271.95
#5	10	50.1	4.1	0.1	1.16	267.62
#6	10	50.1	3.9	0.3	1.22	274.01
#7	10	100	4.0	0.2	1.19	284.78

Each test started with a warm-up stage of the heating zone. Once the temperature values measured by the thermocouples located along the test bench were stabilized, opacity and gas composition values were recorded. A thermophoretic sampling was also taken at this stage. The TEM holder remained in the gas stream for 600 ms, as recommended in a previous study for similar temperature gradients [40]. Such short sampling time is necessary to avoid the presence of overlapping agglomerates on the TEM grids. Furthermore, to ensure that the test bench emissions were effectively stable, duplicates of all measurements — including thermophoretic samplings — were made at 15 min of the initial ones. Those second measures are, therefore, ascertainments of the previous ones.

After this sampling step, A JEOL JEM 1010 transmission electron microscope was used to identify the soot agglomerates previously collected using the thermophoretic system. Micrographs obtained were taken at an acceleration voltage of 100 kV with a 0.35 nm resolution. Magnifications within the range of 25,000 – 40000x were used to achieve successful measurements. Only soot agglomerates with more than three primary particles were considered as fractals at the microscopy stage, and monomers and dimers were excluded [41].

2.3. Processing of TEM micrographs

ImageJ software was used in this step as the digital image processing program.

[26,42]. Once a micrograph has been loaded, a conversion scale from pixels to nanometers is applied according to the magnification used to take the image. A researcher must identify all spherical projections in the agglomerate as primary particles. For this specific study, a researcher trained in TEM microscopy and an operator with no previous experience in carbonaceous structures separately identified the particles inside the agglomerates collected. Therefore, two first estimates of the number of particles were obtained. The diameter of each primary particle ,d_{pp}, was then calculated by averaging the diameters obtained using both the square and circle methods. According to Lee et al. [43], these techniques are based on the circumscription of the identified particles inside simple geometries such as rectangles or circumferences.

After completing all these measurements, statistical tests were carried out to check for normality of size distributions. The tests were selected according to the sample size. Shapiro–Wilk formulation was used for datasets up to 49 values, whereas Kolmogorov–Smirnov with a Lilliefors correction was used for larger datasets.

In addition to information about primary particles, micrographs also provide information about agglomerates. On the one hand, projected surface areas,A_p, are obtainable as a sum of pixels from binary images. On the other hand, a digital analysis allows to sum the distances from the center of gravity to every single pixel occupied by agglomerates and according to Eq. (1), obtain the diameter of gyration, D_g. This size descriptor is defined as the diameter of a circle with the same moment of inertia with respect to their center of gravity as the agglomerate itself [44].

$$D_g = 2\sqrt{\frac{1}{N_{px}}\sum_{k=1}^{N_{px}} |\overrightarrow{r_k} - \overrightarrow{r_c}|^2} \tag{1}$$

where $\overrightarrow{r_k}$ and $\overrightarrow{r_c}$ are position vectors representing the centroid of the agglomerate and the position of the kth pixel respectively, and N_{px} denotes the number of the pixels of the agglomerate.

2.4. Estimation of soot descriptors

Once the image processing described in section 2.3 has been completed, the number of primary particles of each agglomerate can also be estimated as a projected-area derived measurement. This approach to the number of particles from area measurements began with the work carried out by Medalia and Heckman [45], who proposed a power law relationship according to Eq. (2).

$$N_{pp} = \left(\frac{A_p}{a_{pp}}\right)^{\alpha} \tag{2}$$

where a_{pp} is a cross-sectional area assumed representative of the primary particles composing the agglomerate, and α is a constant to account for overlapping effects.

It should be noticed that, as a result of subsequent studies based on simulated aggregates, Köylü et al. [15] proposed an improvement for Eq. (2) by means of Eq. (3).

$$N_{pp} = K_{\alpha}\left(\frac{A_p}{a_{pp}}\right)^{\alpha} \tag{3}$$

Empirical methods determined that K_α and α should be equal to 1.16 and 1.10. More recently, those initial values were refined to 1.15 and 1.09 respectively [46].

Other authors sustain a dependency between the overlapping effect and the irregularity of the agglomerate expressed in terms of fractal dimension, D_f [47]. Therefore, the overlapping factor cannot be a constant exponent and a variable factor z', which replaces α in Eq. (2) was proposed. This exponent is reported to range from as low as $z'_{(D_f=1, N_{pp}=\infty)} = 1$ to as high a $z'_{(D_f=3)} = 1.5$ [47].

However, a recent study based on both computer-generated fractals and experimental measurements has found that this dependency is not excessively significant for particles of $D_f < 2$, determining a value of $z' = 1.059 \pm 0.035$ for Mini-CAST emissions, involving an overestimate of 2% in reported values of D_f [48].

Fractal descriptors can be calculated according to the method proposed by Lapuerta et al. for diesel soot emissions [49,50]. This method, which was already used for experimental research [51], assumes that the number of primary particles can also be computed according to a power law function, as shown in Eq. (4).

$$N_{pp} = K_f\left(\frac{D_g}{d_{pp}}\right)^{D_f} \tag{4}$$

where using Eq. (5), an initial guess of a fractal prefactor, K_f, can be used to refine D_f values until they reach a convergence result which meets the

boundary conditions given by Eq. (6) and Eq. (7), which are based on hypothetical arrangements of primary particles leading to the extreme limits of $1 < D_f < 3$.

$$K_f = K_f(D_f = 1) - 1 + \left(1 + K_f(D_f = 3) - K_f(D_f = 1)\right)^{((D_f-1)/2)^{1.95}} \quad (5)$$

$$K_f(D_f = 1) = \frac{1}{\sqrt{\frac{1}{3} - \frac{1}{N_{pp}} + \frac{8}{5N_{pp}^2}}} \quad (6)$$

$$K_f(D_f = 3) = \frac{\pi}{\sqrt{18}}\left(\frac{5}{3}\right)^{3/2} = 1.593 \quad (7)$$

Lapuerta et al. [49] also provide a dependency between z' and the irregularity of the agglomerate expressed in terms of D_f, given by Eq. (8). Using this equation, z' can be obtained as a variable in the iterative process and, thus, the number of primary particles can be calculated.

$$z' = \frac{lnN_{pp}}{ln(0.8488N_{pp} + 0.1512)} - 1 + \left(2.5 - \frac{lnN_{pp}}{ln(0.8488N_{pp} + 0.1512)}\right)^{((D_f-1)/2)^{1.95}} \quad (8)$$

Therefore, fractal dimension, prefactor and number of primary particles composing the soot agglomerates were characterized according to the five alternatives that are summarized in Table 2.

The use of the diameter of gyration to calculate fractal descriptors according to the procedures described in Table 2 should be emphasized. This diameter is commonly compared with the mobility diameter,D_m, by means of a proportional factor, which typically ranges between $1.29 > D_m/D_g > 0.71$ depending on flow regime and soot size [12]. Mobility diameter is usually considered as a more representative diameter of the soot agglomerate morphology, as it can be compared with experimental results obtained from a DMA. Physically,D_m, is interpreted as the diameter of a sphere with the same electrical mobility as the particle in question. Several research have been focused on mobility diameter calculation for different flow regimes [52]. In this sense, Sorensen [53] concludes that in both continuum and free molecular regimes this mobility diameter is proportional to d_{pp}, and related by a power law to the number of primary particles composing the agglomerate. For the slip transition regime, $0.1 < Kn < 10$, a relation between D_m, d_{pp} and N_{pp} is also given [53]:

$$D_m = d_{pp}\left(10^{-2x+0.92}\right)N_{pp}^{x}, N_{pp} \geq 100 \quad (9)$$

$$D_m = d_{pp}N_{pp}^{0.46}, N_{pp} < 100 \quad (10)$$

where x is suggested to be described as $x = 0.51Kn^{-0.043}$ [26]. Authors such as De Carlo et al. [47] also attach importance to the way in which the dynamic shape factor, which is the ratio between the drag force on a real particle and the resistance force on its equivalent sphere, varies as a function of the aggregate size. For this characterization, this dynamic shape factor was estimated from the number of primary particles according to the two regimes indicated in Eq. (11), [54].

Table 2
Methods used to calculate fractal descriptors and number of primary particles.

Calculation alternative	*N_{pp} calculation process*	*D_f and K_f calculation process*
A	Manual counting by an inexperienced operator	*Eq.*(4)&*Eq.*(5)
B	Manual counting by an expert operator	*Eq.*(4)&*Eq.*(5)
C	It is calculated iteratively with D_f and K_f considering z' in Eq. (2)	*Eq.*(4),*Eq.*(5)&*Eq.*(8)
D	$Eq.(2)\,|_{\alpha=1.059}$	*Eq.*(4)&*Eq.*(5)
E	$Eq.(3)\,|_{K_a=1.15\&\alpha=1.09}$	*Eq.*(4)&*Eq.*(5)

$$\chi = \begin{cases} N_{pp}^{0.11}, N_{pp} < 60 \\ 0.6N_{pp}^{0.24}, N_{pp} \geq 60 \end{cases} \quad (11)$$

Furthermore, the relationship between electrical mobility diameter and the volume equivalent diameter, D_{ve} — diameter of a sphere with the same volume as the agglomerate — can be obtained by equating the drag force in terms of D_m to that in terms of χ and D_{ve}. This process leads, for the transition regime, to the expression presented in Eq. (12) [54].

$$\chi = \frac{D_m}{D_{ve}}\frac{C(D_{ve})}{C(D_m)} \quad (12)$$

where $C(D)$ is the Cunningham slip correction factor for the agglomerate size, whose presence involves a correction to account the reduction in drag that occurs when the relative velocity of the gas at the particle surface is not null.

In addition, the total volume of an agglomerate can be simply calculated via multiplication of number of constituent particles by the volume of a single primary particle [44]. Therefore, mass of soot agglomerates can be estimated by Eq. (13).

$$m = N_{pp}\rho_{pp}\pi\frac{d_{pp}^3}{6} \quad (13)$$

where ρ_{pp} is the material density of the primary particles constituting the soot core. An approximate value of 2 g/cm^3 for onion-like structures made from parallel graphene sheets, was suggested by previous research [55,56]. Authors such as De Carlo et al. [47] also define an effective density, ρ_{eff}, as the density that a sphere with diameter D_m would need to have the same mass as the actual agglomerate as given by Eq. (14).

$$m = \frac{\rho_{eff}\pi D_m^3}{6} \quad (14)$$

Finally, from mass and standard density,$\rho_0 = 1\mathrm{g/cm^3}$, the aerodynamic diameter D_a — defined as the diameter of a sphere with a standard density that settles at the same terminal velocity as the particle of interest — can be calculated according to Eq. (15). This diameter is also commonly used for characterization purposes, as it can be compared from experimental results obtained from aerodynamic classifiers such as cascade impactors [57].

$$D_a = \left(\frac{6m}{\rho_0\pi}\right)^{1/3} \quad (15)$$

3. Results and discussion

3.1. Gas measurements

Fig. 3 summarizes the gas composition of the exhaust streams generated for the operating conditions indicated in Table 1. Measurements performed using the gas analyzer involve higher percentages of O_2 and lower levels of CO_2 compared to those values expected for engine emissions [58]. This fact is due to the influence of the dilution air conditions. Operating conditions (5) and (6), which involve the lowest levels of dilution air, also involve the highest percentages of combustion products detected, as well as the lowest volume of oxygen.

As expected, it was also observed that an increase in the richness of the gas mixture involves a reduction in the incomplete combustion products composing the exhaust stream. The combined effect of the Mini-CAST flow rate conditions was statistically evaluated. Fig. 4 shows a graphic depiction of the regressions obtained in terms of dilution air flow and equivalence ratio (Φ), As it can be seen, an increase in the equivalence ratio favors the formation of CO molecules at the expense of the CO_2 concentration. Same trend was also found for HC concentrations.

Opacimeter measurements, quantified by the filter smoke number

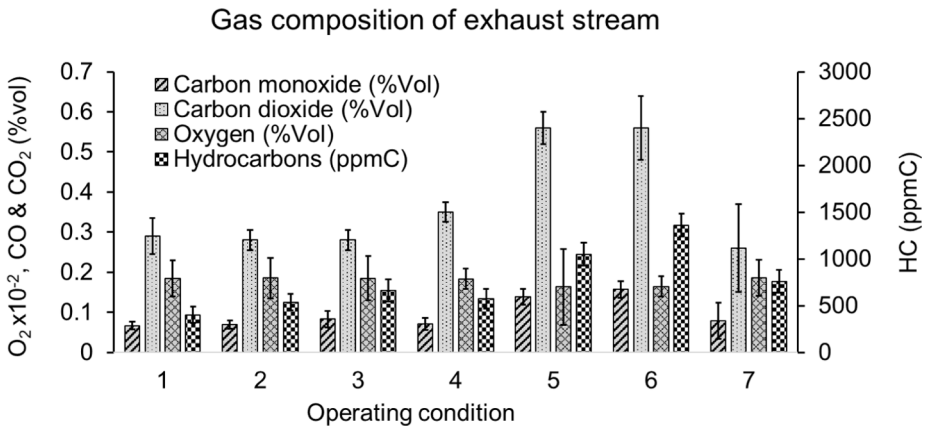

Fig. 3. Gas composition of the exhaust stream. Error bars denote the standard deviations between consecutive readings of the measuring devices.

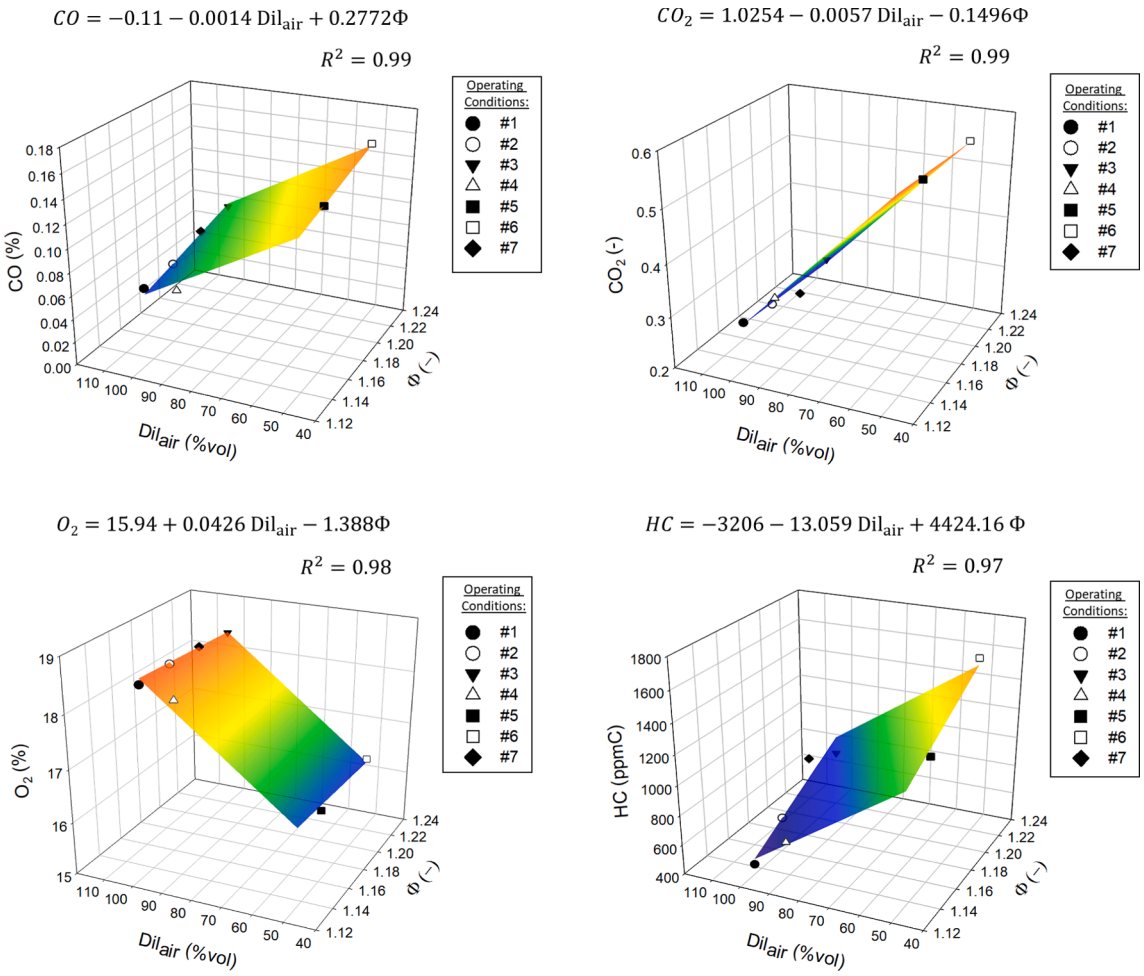

Fig. 4. Composition of the exhaust gas stream as function of the dilution air rate ($\mathrm{Dil_{air}}$) and the equivalence ratio (Φ). The colored curves denote the fitting planes.

(FSN), were also evaluated in terms of the test bench conditions (see Fig. 5). Composition of the oxidizing agent has been found as the most significant factor regarding opacity results. This influence involves two different effects. On the one hand, an increase of the N_2 mixing flow dilutes the concentration of particles. On the other hand, a reduction of the oxidizing O_2 flow worsens the quality of the combustion involving greater particle concentrations.

3.2. Examples of soot agglomerates

In order to illustrate the TEM results obtained from the microscopy stage, micrographs selected to represent the average properties of soot agglomerates of each operating condition are shown in Fig. 6. A total of 350 agglomerates were identified during the microscopy stage, whereas 1742 primary particles were counted. Fig. 6 also specifies the number of agglomerates analyzed per operating condition, where large variations in the geometry and size of the soot particulate were visually observed

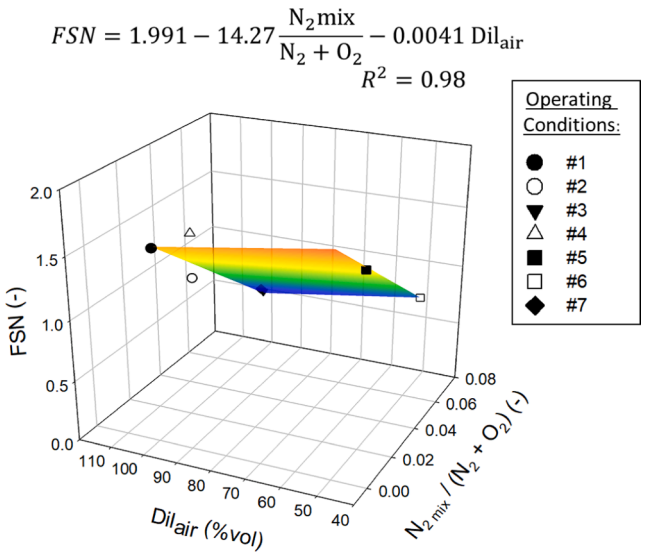

Fig. 5. Relationship between FSN and burner settings. The colored curve denotes the fitting plane.

under the microscope: Whereas micrographs of conditions 1-2-3-6-7 show smaller agglomerates, greater agglomerates can be seen for the micrographs of conditions (4) and (5).

3.3. Primary particles diameters

The analysis of the primary particles, which were previously identified by TEM inspection, was conducted. Fig. 7a summarizes the distributions of the diameters found for each pair of samples of each operating condition.

It was detected that all those distributions range between similar limits. It was also confirmed that those limits are comparable with size ranges reported by primary particles generated by other sources such as diesel engines, diffusion flames and other burner-based facilities (see Fig. 7b). In fact, considering the total amount of the 1742 particles identified, a mean diameter and a standard error equal to 23.02 ± 0.16 nm were found. It was also confirmed that this mean diameter is comparable with mean values reported for engine exhaust emissions (25 nm), ethylene turbulent flames (10–35 nm), co-flow burners (20–40 nm) and other experimental setups based on CAST burners (19.7 nm) [13,55,64,65].

Despite the small differences observed in Fig. 7a, primary particles seem to be slightly affected by the combustion modes. As it can be seen in Fig. 8, the size of the primary particles should decrease by increasing the dilution air and the N_2 flow rate. This observation was also reported by Yahia et al. [63], who found changes from 22.7 nm to as low as 14.5

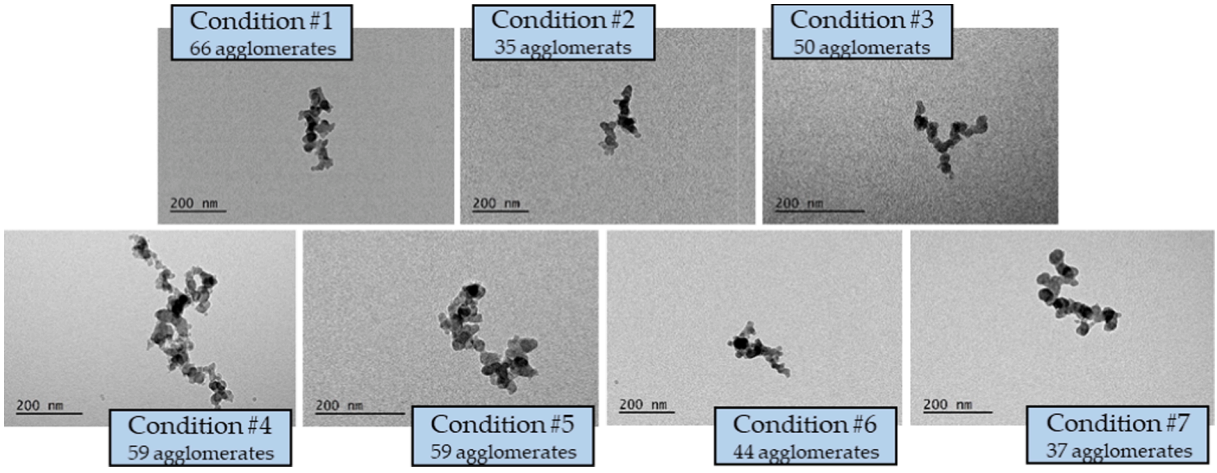

Fig. 6. Examples and number of soot agglomerates captured for each operating condition.

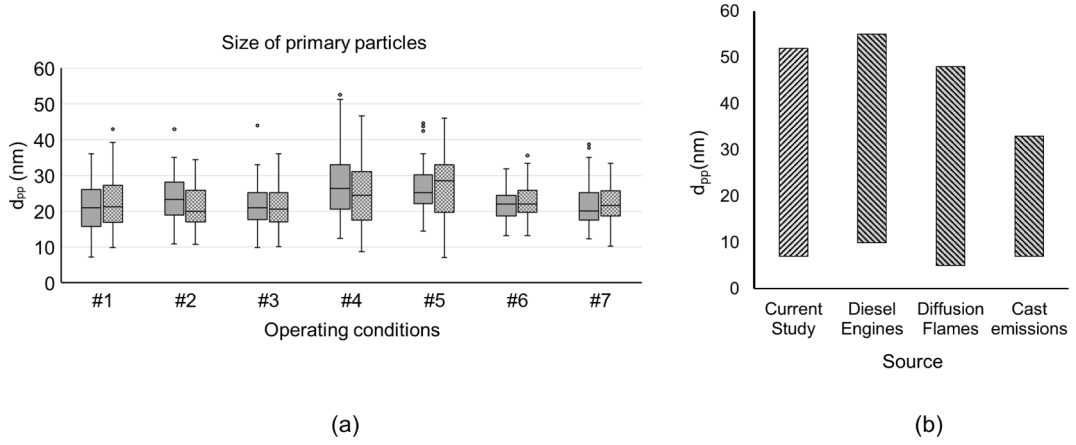

Fig. 7. (a) Boxplots of diameters of primary particles for each operating condition; **(b)** Comparison of d_{pp} values in this study with other sources from literature: diesel engines [49,59], diffusion flames [20,60–62], and Mini-Cast burner [63].

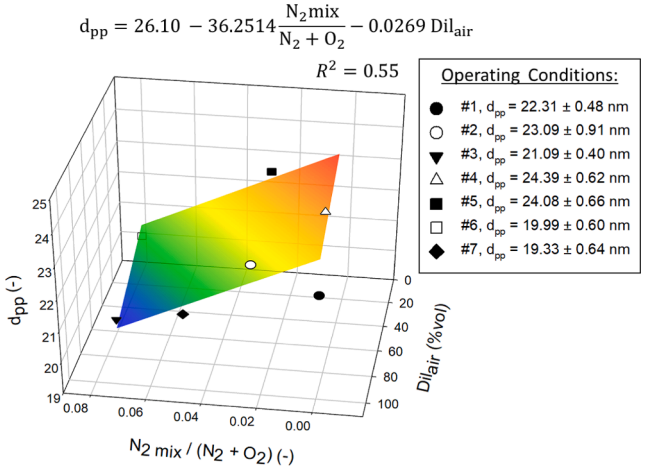

Fig. 8. Relations between primary particles diameters and test bench setting conditions. Mean d_{pp} values are shown accompanied by standard errors according to Gilmore [67]. The colored curve denotes the fitting plane.

nm as the N_2 mixing flow increases. This effect may be due to a shorter residence time of the particulate generated in the zone where nucleation occurs [66]. It is also possible that increasing nitrogen flow actually dilutes the particle precursors in the gas phase that were produced in the flame, subsequently reducing the size of the primary particles and hindering the growth of existing soot nuclei.

In support of this contention, a statistical analysis of the diameters of the primary particles was conducted. The normality tests depicted that, with a high level of confidence (>90%), size distributions can be approximated by normal distributions. Furthermore, an ANOVA test confirmed that the diameter of the primary particles can be influenced by the specific conditions of each experimental test, with a p-value greater than 0.05.

3.4. Size of soot agglomerates

3.4.1. Diameters of gyration and projected areas

Fig. 9a summarizes the mean diameters of gyration and projected areas found for the different operating conditions. It was observed that both descriptors, A_p and D_g, show similar trends. This similarity was also reported by Lapuerta et al. [22], as both parameters are direct indicators of the size of the soot agglomerates.

Unlike primary particles, whose diameters slightly depend on the operating conditions, a strong influence of the burner settings can be observed considering the size of the soot agglomerates. It seems that a greater dilution air flow, which decreases particulate concentration, leads to agglomerates of lesser size. This effect can be due to a reduction in the probability for collisions and agglomeration to occur. In fact, a similar observation was also reported due to a shorter residence time, on a study of the effects of diesel engine conditions on the size of soot emissions [68].

3.4.2. Number of primary particles

The number of primary particles composing each agglomerate was evaluated considering the five calculation alternatives described in Section 2.4 (see Fig. 10). Before analyzing the influence of the operating conditions on the number of those primary particles, it should be noted that significant differences have been found between the characterization methodologies used. Manual counting methods (alternatives A and B) involve smaller agglomerates than those obtained assuming projected-area derived measurements (alternatives C, D and E). Furthermore, both the expert researcher and the inexperienced one, carried out counts that culminated in agglomerates with overlapping exponents less than unity, which lacks a sense as those overlapping values would imply the absence of physical contact between primary particles.

It was also detected that distributions obtained as derived measurements (alternatives C, D and E) are practically equivalent, where differences between alternatives seems to increase as the size of the agglomerates increases. This fact may be due to the increasing influence of the overlapping exponent as the size of the particulate increases. Therefore, distributions composed by larger agglomerates could show greater variability between methods.

A statistical analysis was performed to support this contention by means of Mann-Whitney Rank tests. Significant differences between median values obtained by both human inspections were found (U-statistic equal to 15636.50). In contrast, there are no statistically significant differences between distributions obtained according to the approaches reported by literature, where the maximum similarity was found between alternatives C and D (overlapping exponent, z' and relation proposed by Köylü et al. [15] respectively) with a U-statistic equal to 124107.

The influence of the test conditions on the number of primary particles was also statistically analyzed. Fig. 9b summarizes the relations found considering an overlapping exponent, z' (alternative C). It was detected that the number of primary particles was significantly affected by the operating conditions (p-value $\gg$ 0.05). As it also was observed in Section 3.4.1, it seems that a greater dilution air flow leads on agglomerates composed by a lesser number of primary particles and therefore, on agglomerates of lesser size (see Fig. 9b). Similarly, lower

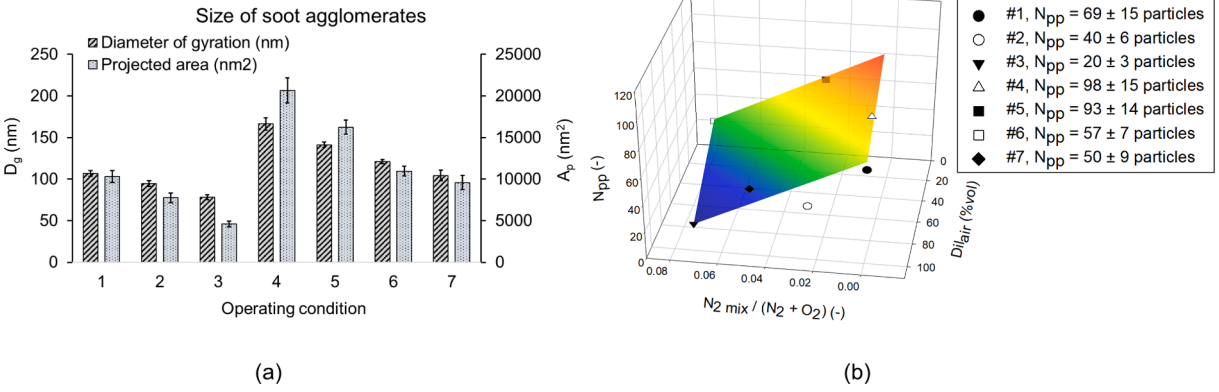

Fig. 9. (a) Size of soot agglomerates according to each operating condition. Error bars depict standard errors [67]; **(b)** Relation between mean number of primary particles and burner conditions for a variable z' (alternative C). The colored curve denotes the fitting plane and mean values are given along with standard errors.

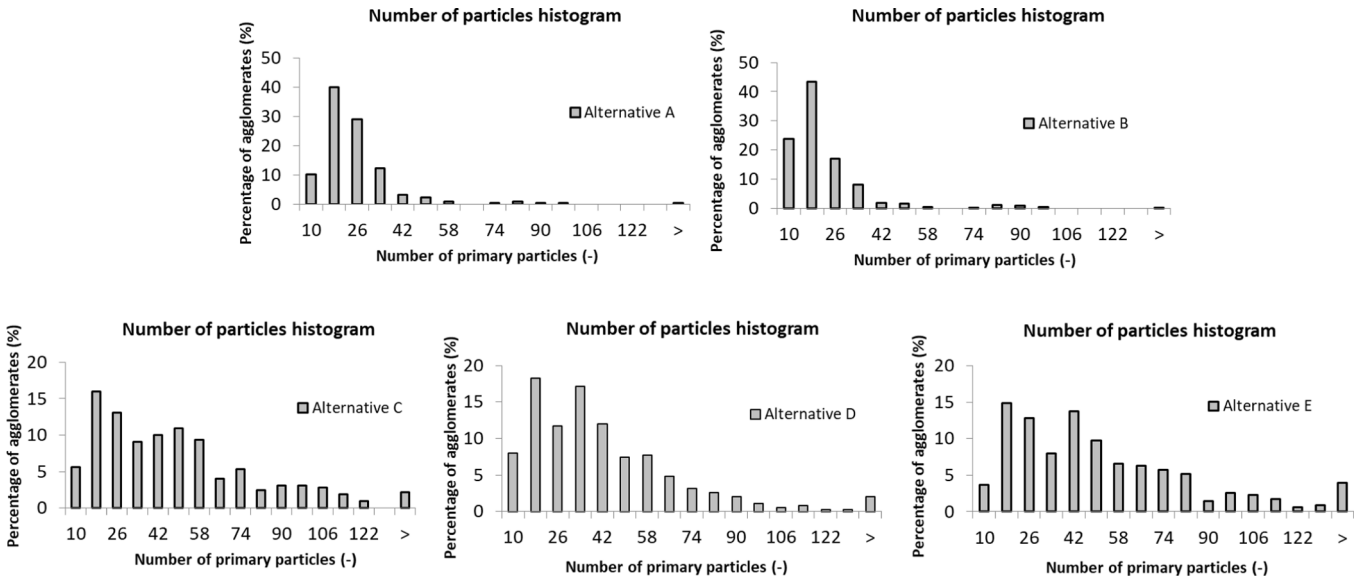

Fig. 10. Number of primary particles. Comparison between fractal approaches considered.

mixing flows, which are related with lower residence times in the burner, seem to result in an increase in the aggregate size. This observation agrees with previous experimental studies, where a similar trend was found by means of Scanning Mobility Particle Sizer (SMPS) measurements [63].

3.4.3. Mobility diameters

Mobility diameters were calculated considering each of the five distributions of primary particles previously obtained. Linear relationships between D_g and D_m are shown in Fig. 11, where differences between characterization methods are evident. It was detected that manual inspection procedures (alternatives A and B) involve greater data dispersion than projected-area derived measurements (alternatives C, D and E). As it can be seen from Fig. 11, manual processes result in Pearson's coefficients <0.1, whereas values greater than 0.6 were found for the other three alternatives. Furthermore, deficiencies of manual counting methods are evident. Ratios around $D_m/D_g \approx 3$ were found for alternatives A and B, whereas values expected according to Sorensen [53] should fulfill that $D_m/D_g < 1.29$.

By contrast, distributions found considering the overlapping functions reported by literature are coherent with the proportionality relations described by Sorensen [53]. It has to keep in mind that mobility diameters were calculated using Eq. (9) for agglomerates composed of <100 particles and using Eq. (10) for greater agglomerates. In this sense, it was detected that those three approaches — C, D and E —, are almost equivalent for smaller agglomerates, whereas greater differences were found around 100 monomers composing the particles.

In support of this contention, a statistical analysis of those results was conducted. Although differences between the overlapping function approaches (alternatives C, D and E) increase as the agglomerates grow, those differences were not significant enough to fail a sum rank test. Therefore, those distributions can be assumed as equivalents.

3.5. Fractal dimension

The study of the fractal dimension of the agglomerates collected confirms some tendencies, which were detected at the TEM analysis stage. Fig. 12 summarizes the fractal dimensions obtained, where significant differences have been found between the five characterization alternatives considered. It was discovered that manual counting methods (alternatives A, B) involve greater data dispersion than the other three alternatives considered in this work — C, D and E —.

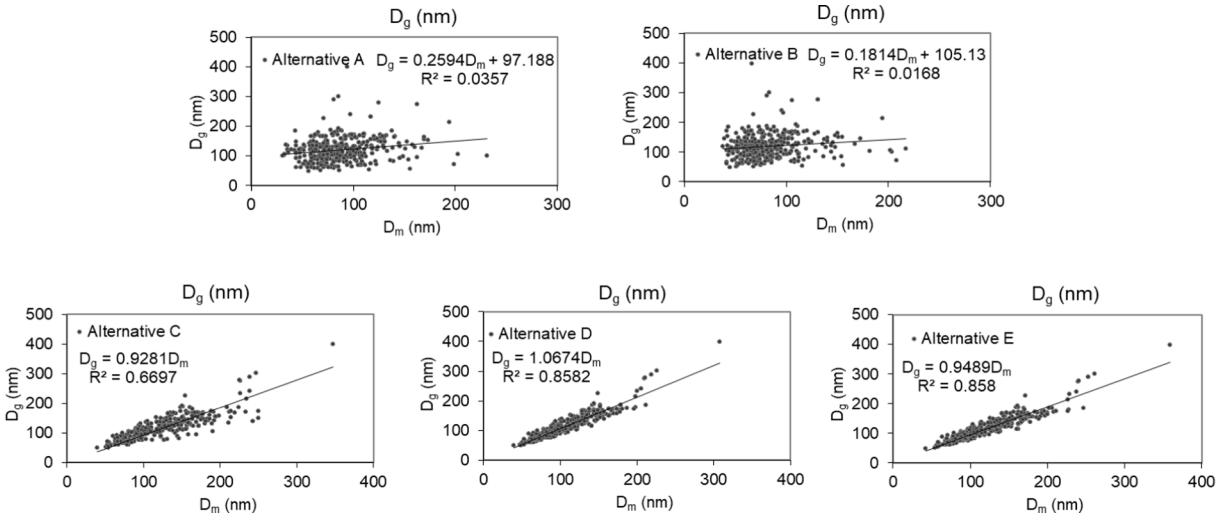

Fig. 11. Relations between D_g and D_m for the five approaches considered.

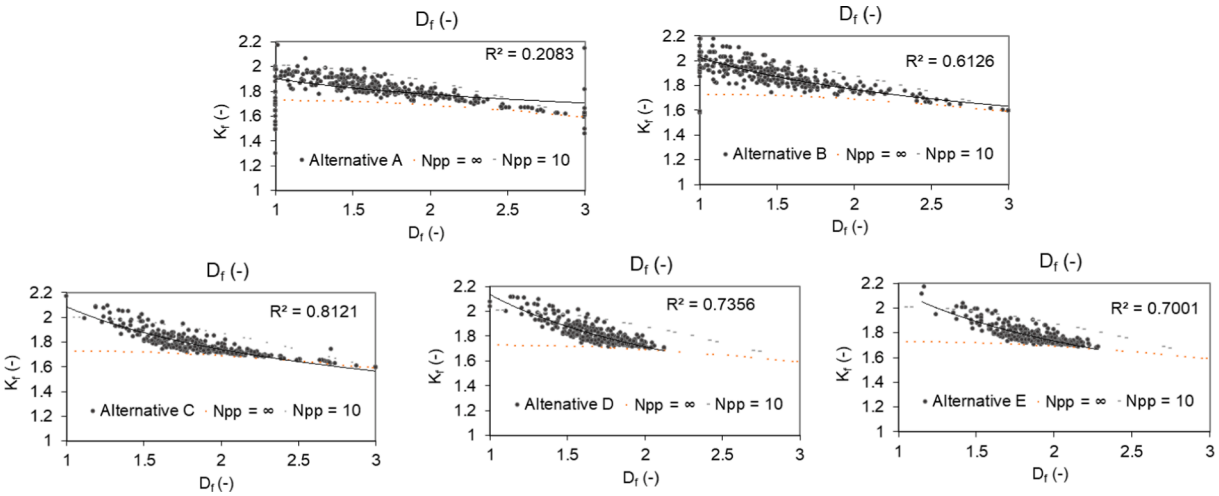

Fig. 12. Comparative of fractal descriptors among the five approaches considered. Green and red lines show the theoretical values for a dozen and an infinite number of particles.

Furthermore, an underestimation of the number of particles counted by the human inspections can lead to inconsistencies regarding D_f and K_f boundary conditions.

Results obtained using the equation proposed by Köylü et al. [15] and assuming an overlapping exponent, z' (alternatives D and C) are almost equivalent, with mean values of $D_f = 1.87 \pm 0.01$ and $D_f = 1.90 \pm 0.02$, respectively. Greater differences have been found assuming a constant exponent factor from Mini-CAST literature (alternative D and $D_f = 1.70 \pm 0.01$), which tends to reduce the fractal values. Those observations have been statistically probed, with a p-value equal to 0.23 on rank sum tests.

A statistical analysis of the influence of the operating conditions on the fractal dimensions obtained through alternative C, was performed. A p-value greater than 0.05 suggests a significant relation between D_f and both dilution air and N_2 flow conditions (see Fig. 13a). In fact, an increase of the N_2 mixing flow seems to imply a lower possibility of agglomeration, which involves less compact structures, and therefore a lower D_f. Furthermore, as it can be seen from Fig. 13b, it was also confirmed that the fractal dimensions obtained in this research are comparable with results reported by previous studies focused on CAST emissions, diesel engines and diffusion flames.

3.6. Mass and effective density

Mass and effective densities were calculated for each agglomerate examined at the microscopy stage. Thus, the characteristic mass-mobility relationship of the soot generation bench was identified. Those results are summarized in Fig. 14, where an increase in the soot masses occurs owing to an increase in the mobility diameters. As it can also be seen, those relationships can be described through a power law function, with a Pearson's correlation coefficient greater than 0.90 for all alternatives.

Those mass-mobility exponents range between 2.24 and 2.48 depending on the calculation method used. Those values are in the range of the exponents reported by other researchers regarding diffusion burners (1.9 ± 0.1) and aircraft engines (1.85–2.79) [74,75]. Alternatives C, D and E lead to similar mass values, which are slightly greater than those values obtained from manual counting processes (alternatives A and B).

From Fig. 15, as particles befits agglomerate structures, effective

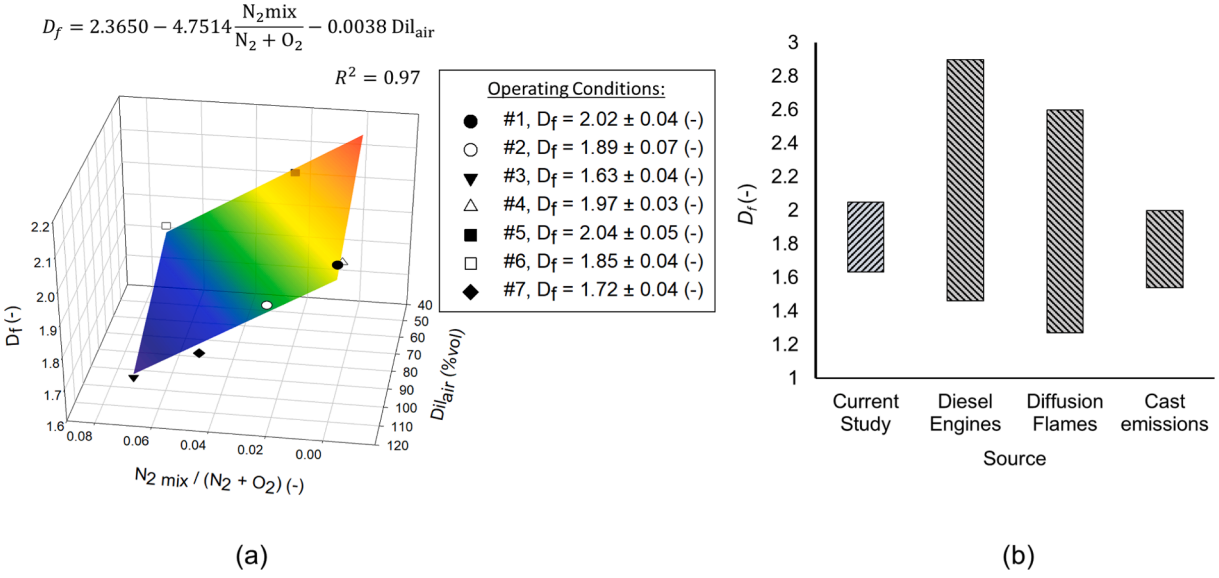

Fig. 13. (a) Fractal dimension relationships regarding burner conditions. Standard errors were considered for mean values; **(b)** Comparative of mean fractal dimensions obtained among values reported for Mini-Cast emissions [63], diesel engines [69–71] and diffusion flames [62,72,73].

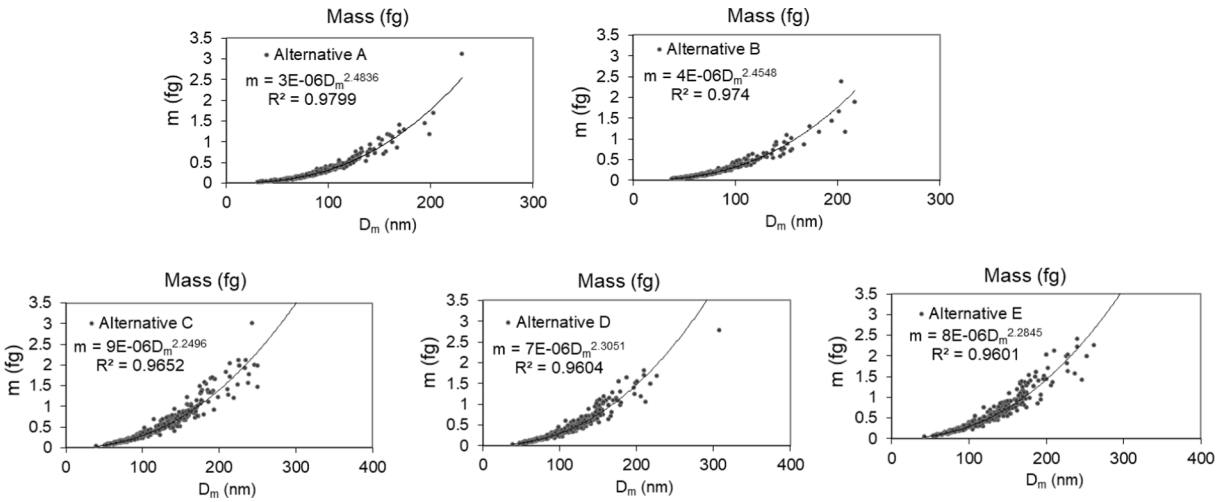

Fig. 14. Comparison of mass values between the five approaches considered.

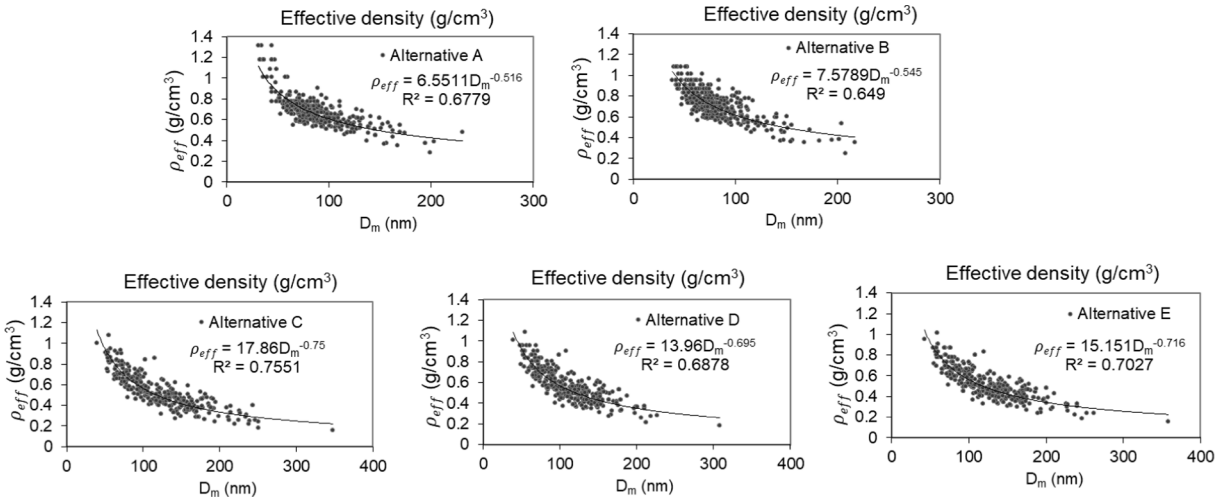

Fig. 15. Effective densities found considering each alternative.

densities decreased with increasing D_m from around 1.2 g/cm^3 at 50 nm to as low as approximately 0.2 g/cm^3 at 380 nm. Furthermore, Fig. 16 shows a comparison between mean effective densities found according to calculation alternative C (considering the overlapping exponent as a variable) and results reported for different emissions sources. Effective densities obtained in this study seem to be aligned on the same trend. This is probably because primary particles obtained in the present study have similar mean diameters among all operating conditions. It was also confirmed that the effective densities of the agglomerates examined are comparable with those produced by both engine and CAST emissions [26,76].

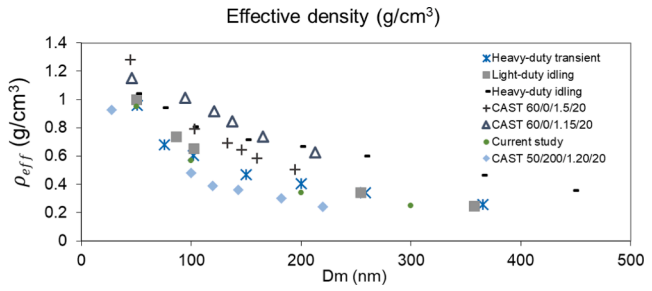

Fig. 16. Effective density vs mobility diameter. Results of the current study are compared to values obtained for engines and for CAST emissions [26,76].

3.7. Shape factor, aerodynamic and volume equivalent diameter

Fig. 17 shows results of the shape factor obtained according to each of the five calculation methods considered. Shape factors which are closed to unity involves compact and nearly spherical particulates, whereas larger values of χ imply particulates that deviate significantly from a sphere. It was also confirmed that all those results agree with values reported by Park et al. [69], in whose experimental research the shape factor increases from 1.11 to 2.21 as the soot size increases from 50 nm to 220 nm. However, despite the slight differences observed between the calculation alternatives C, D and E, the manual counting processes (alternatives A and B) show again greater discrepancies than expected.

Similar contention can be inferred from Fig. 18a and Fig. 18b, where relationships found between D_m, D_a and D_{ve} are shown for calculation alternative C (considering the overlapping exponent as a variable). Agglomerates of mobility diameters around 50 nm satisfies that $D_m \approx D_{ve}$. Therefore, those agglomerates involve compact structures with internal voids [47]. However, as the aggregates increase in size, the gap between those two diameters increases, resulting in irregular agglomerates that mostly have no internal voids.

Furthermore, the aerodynamic diameter tends to increase as the

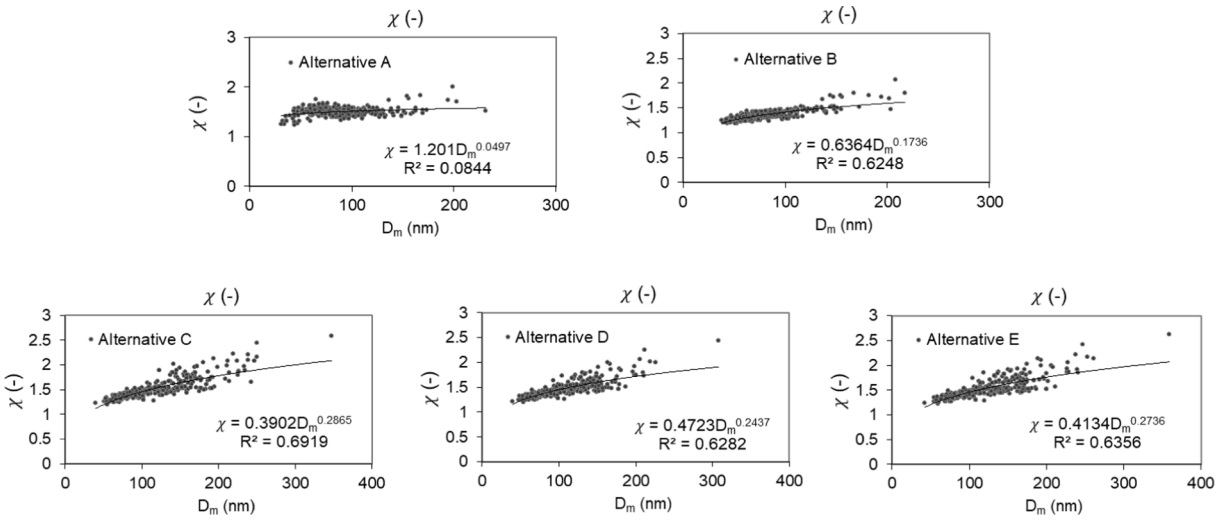

Fig. 17. Shape factor vs mobility diameter.

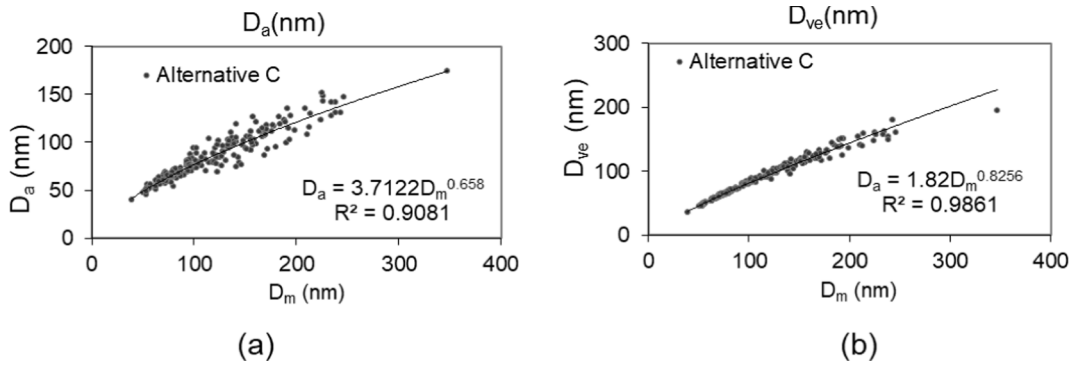

Fig. 18. (**a**) Aerodynamic vs mobility diameter according to calculation alternative C; **(b)** Volume equivalent diameter vs mobility diameter according to calculation alternative C.

mobility diameter increases. It must be kept in mind that an irregular particle of unitary density should fulfill that $D_a < D_{ve} < D_m$. However, as relations of $\rho/\chi > 1$ can be found for this dataset, ratios such as $D_a/D_{ve} > 1$ are also consistent with previous studies [47].

4. Conclusions

In this study, soot agglomerates emitted by a combustion aerosol generation bench were characterized according to their size, mass, and fractal behavior. To achieve this aim, synergies between thermophoretic sampling and TEM microscopy were successfully applied. Seven different operating conditions were considered. From the micrograph inspection of the agglomerates generated through those operating conditions, non-significant differences in mean diameter values were detected for primary particles. In contrast, the diameters of gyration, number of primary particles and projected areas mainly depend on the composition of the oxidizing agent. Concentrations of N_2 and O_2 that involve the generation of a greater volume of particles leads to agglomerates of greater size. Fractal dimension has also been found highly dependent on the composition of the oxidizing mixture, where greater fractal dimension values were found for operating conditions of greater concentration.

Significant differences between manual counting processes and the use of overlapping functions reported by literature were found in terms of the number of primary particles. Those manual counting processes tend to underestimate the number of particles involving overlapping exponents less than unity. Number of primary particles obtained combining the formulations proposed by Köylü and Lapuerta were found equivalent.

Based on the fractal theory, an approach has been used for approximate mobility diameters and, therefore, mass and effective density values. In this sense, an increase in the mobility diameter involves a decrease in the effective density, whereas mass values show the opposite trend. The irregularity of the agglomerates was also observed in terms of the dynamic shape factor. This factor has been found to tend to increase for particulates of greater mobility diameter and, therefore, smaller effective density.

Overall, results obtained in this study allow a deeper understanding of the combustion aerosol properties and, in future studies, this work will be complemented with in-situ readings of aerodynamic and mobility diameters.

CRediT authorship contribution statement

Concepción Paz: Conceptualization, Formal analysis, Supervision, Writing – original draft, Writing – review & editing, Resources, Project administration. **Adrián Cabarcos:** Methodology, Formal analysis, Data curation, Investigation, Software, Validation, Visualization, Writing – original draft, Writing – review & editing. **Marcos Conde:** Software, Validation, Writing – review & editing. **Christian Gil:** Data curation, Validation, Writing – review & editing.

Declaration of Competing Interest

The authors declare that they have no known competing financial interests or personal relationships that could have appeared to influence the work reported in this paper.

Acknowledgment

This research was funded by the Spanish Ministry of Science and Innovation through the ENE2017-87855-R project.

References

[1] R. Dastanpour, S.N. Rogak, B. Graves, J. Olfert, M.L. Eggersdorfer, A.M. Boies, Improved sizing of soot primary particles using mass-mobility measurements, Aerosol Sci. Technol. 50 (2016) 101–109, https://doi.org/10.1080/02786826.2015.1130796.

[2] S. Baldacci, S. Maio, S. Cerrai, G. Sarno, N. Baïz, M. Simoni, I. Annesi-Maesano, G. Viegi, Allergy and asthma: effects of the exposure to particulate matter and biological allergens, Respir. Med. 109 (2015) 1089–1104, https://doi.org/10.1016/j.rmed.2015.05.017.

[3] G.B. Hamra, N. Guha, A. Cohen, F. Laden, O. Raaschou-Nielsen, J.M. Samet, P. Vineis, F. Forastiere, P. Saldiva, T. Yorifuji, D. Loomis, Outdoor Particulate Matter Exposure and Lung Cancer: A Systematic Review and Meta-Analysis, Environ. 122 (2014) 906–911. https://ehp.niehs.nih.gov/doi/abs/10.1289/ehp/1408092.

[4] C.A. Pope III, D.W. Dockery, Health effects of fine particulate air pollution: lines that connect, J. Air Waste Manage. Assoc. 56 (2006) 709–742, https://doi.org/10.1080/10473289.2006.10464485.

[5] A.E. Torkayesh, R. Alizadeh, L. Soltanisehat, S.E. Torkayesh, P.D. Lund, A comparative assessment of air quality across European countries using an integrated decision support model, Socio-Econ. Plan. Sci. (2021), 101198, https://doi.org/10.1016/j.seps.2021.101198.

[6] E. Mattarelli, C. Rinaldini, P. Patroncini, Commercial vehicles: new diesel engine concepts for Euro VI and beyond, SAE Tech. Pap. (2017), https://doi.org/10.4271/2017-26-0034.

[7] N. Hooftman, M. Messagie, J.V. Mierlo, T. Coosemans, A review of the European passenger car regulations – real driving emissions vs local air quality, Renew. Sust. Energ. Rev. 86 (2018) 1–21, https://doi.org/10.1016/j.rser.2018.01.012.

[8] G. Okyay, E. Héripré, T. Reiss, P. Haghi-Ashtiani, T. Auger, F. Enguehard, Soot aggregate complex morphology: 3D geometry reconstruction by SEM tomography applied on soot issued from propane combustion, J. Aerosol Sci. 93 (2016) 63–79, https://doi.org/10.1016/j.jaerosci.2015.11.009.

[9] S.K. Choi, B.C. Choi, S.M. Lee, J.H. Choi, The effect of liquid fuel doping on PAH and soot formation in counterflow ethylene diffusion flames, Exp. Therm Fluid Sci. 60 (2015) 123–131, https://doi.org/10.1016/j.expthermflusci.2014.08.008.

[10] D. Patiño, R. Pérez-Orozco, J. Porteiro, M. Lapuerta, Characterization of biomass PM emissions using thermophoretic sampling: composition and morphological description of the carbonaceous residues, J. Aerosol Sci. 127 (2019) 49–62, https://doi.org/10.1016/j.jaerosci.2018.10.005.

[11] C. Jäger, T. Henning, R. Schlögl, O. Spillecke, Spectral properties of carbon black, J Non Cryst Solids. 258 (1999) 161–179, https://doi.org/10.1016/S0022-3093(99)00436-6.

[12] M.M. Maricq, N. Xu, The effective density and fractal dimension of soot particles from premixed flames and motor vehicle exhaust, J. Aerosol Sci. 35 (2004) 1251–1274, https://doi.org/10.1016/j.jaerosci.2004.05.002.

[13] J.-O. Müller, D.S. Su, R.E. Jentoft, U. Wild, R. Schlögl, Diesel engine exhaust emission: oxidative behavior and microstructure of black smoke soot particulate, Environ. 40 (2006) 1231–1236, https://doi.org/10.1021/es0512069.

[14] A.M. Brasil, T.L. Farias, M.G. Carvalho, A recipe for image characterization of fractal-like aggregates, J. Aerosol Sci. 30 (1999) 1379–1389, https://doi.org/10.1016/S0021-8502(99)00026-9.

[15] Ü.Ö. Köylü, G.M. Faeth, T.L. Farias, M.G. Carvalho, Fractal and projected structure properties of soot aggregates, Combust. Flame 100 (1995) 621–633, https://doi.org/10.1016/0010-2180(94)00147-K.

[16] M.N. Ess, K. Vasilatou, Characterization of a new miniCAST with diffusion flame and premixed flame options: generation of particles with high EC content in the size range 30 nm to 200 nm, Aerosol Sci. Technol. 53 (2019) 29–44, https://doi.org/10.1080/02786826.2018.1536818.

[17] A. Mamakos, I. Khalek, R. Giannelli, M. Spears, Characterization of combustion aerosol produced by a mini-CAST and treated in a catalytic stripper, Aerosol Sci. Technol. 47 (2013) 927–936, https://doi.org/10.1080/02786826.2013.802762.

[18] A.E. Karataş, Ö.L. Gülder, Soot formation in high pressure laminar diffusion flames, Prog. Energy Combust. Sci. 38 (2012) 818–845, https://doi.org/10.1016/j.pecs.2012.04.003.

[19] R. Dobbins, C. Megaridis, Morphology of flame-generated soot as determined by thermophoretic sampling, Langmuir 3 (1987) 254–259, https://doi.org/10.1021/la00074a019.

[20] F.X. Ouf, J. Yon, P. Ausset, A. Coppalle, M. Maillé, Influence of sampling and storage protocol on fractal morphology of soot studied by transmission electron microscopy, Aerosol Sci. Technol. 44 (2010) 1005–1017, https://doi.org/10.1080/02786826.2010.507228.

[21] A.J. Hurd, W.L. Flower, In situ growth and structure of fractal silica aggregates in a flame, J. Colloid Interface Sci. 122 (1988) 178–192, https://doi.org/10.1016/0021-9797(88)90301-3.

[22] M. Lapuerta, J. Barba, A.D. Sediako, M.R. Kholghy, M.J. Thomson, Morphological analysis of soot agglomerates from biodiesel surrogates in a coflow burner, J. Aerosol Sci. 111 (2017) 65–74, https://doi.org/10.1016/j.jaerosci.2017.06.004.

[23] P.H. McMurry, X. Wang, K. Park, K. Ehara, The relationship between mass and mobility for atmospheric particles: a new technique for measuring particle density, Aerosol Sci. Technol. 36 (2002) 227–238, https://doi.org/10.1080/027868202753504083.

[24] S.W. Stein, B.J. Turpin, X. Cai, P.-F. Huang, P.H. Mcmurry, Measurements of relative humidity-dependent bounce and density for atmospheric particles using the DMA-impactor technique, Atmospheric Environ. 28 (1994) 1739–1746, https://doi.org/10.1016/1352-2310(94)90136-8.

[25] B.K. Ku, P. Kulkarni, Application of fractal theory to estimation of equivalent diameters of airborne carbon nanotube and nanofiber agglomerates, Aerosol Sci. Technol. 52 (2018) 597–608, https://doi.org/10.1080/02786826.2018.1441974.

[26] J. Rissler, M.E. Messing, A.I. Malik, P.T. Nilsson, E.Z. Nordin, M. Bohgard, M. Sanati, J.H. Pagels, Effective density characterization of soot agglomerates from various sources and comparison to aggregation theory, Aerosol Sci. Technol. 47 (2013) 792–805, https://doi.org/10.1080/02786826.2013.791381.

[27] A. Moallemi, M. Kazemimanesh, J.C. Corbin, K. Thomson, G. Smallwood, J. S. Olfert, P. Lobo, Characterization of black carbon particles generated by a propane-fueled miniature inverted soot generator, J. Aerosol Sci. 135 (2019) 46–57, https://doi.org/10.1016/j.jaerosci.2019.05.004.

[28] A. Keller, T. Tritscher, H. Burtscher, Performance of water-based CPC 3788 for particles from a propane-flame soot-generator operated with rich fuel/air mixtures, J. Aerosol Sci. 60 (2013) 67–72, https://doi.org/10.1016/j.jaerosci.2013.02.005.

[29] H. Burtscher, Comparison of particle emissions from different combustion systems, J. Aerosol Sci. 31 (2000) 620–621, https://doi.org/10.1016/S0021-8502(00)90629-3.

[30] C. Paz, E. Suárez, J. Vence, A. Cabarcos, Fouling evolution on ribbed surfaces under EGR dry soot conditions: experimental measurements and 3D model validation, Int. J. Therm. Sci. 151 (2020), 106271, https://doi.org/10.1016/j.ijthermalsci.2020.106271.

[31] C. Paz, E. Suárez, J. Vence, J. Hoard, Evolution of EGR cooler deposits under hydrocarbon condensation: analysis of local thickness, roughness, and fouling layer density, Int. J. Therm. Sci. 161 (2021), 106744, https://doi.org/10.1016/j.ijthermalsci.2020.106744.

[32] L. Jing, Standard Combustion Aerosol Generator (SCAG)for Calibration Purposes, in: 3rd ETH Workshop "Nanoparticle Measurement", ETH Hönggerberg Zürich, 1999.

[33] E. Barthazy, O. Stetzer, C. Derungs, H. Saathoff, U. Lohmann, Water uptake of soot particles emitted from a Jing-CAST soot generator, in: 12th Conference Cloud Physics, 2006.

[34] D. Grondin, P. Breuil, J.P. Viricelle, P. Vernoux, Development of a particulate matter sensor for diesel engine, Procedia Eng. 120 (2015) 1237–1240, https://doi.org/10.1016/j.proeng.2015.08.838.

[35] R. Moore, L. Ziemba, D. Dutcher, A. Beyersdorf, K. Chan, S. Crumeyrolle, T. Raymond, K. Thornhill, E. Winstead, B. Anderson, Mapping the operation of the miniature combustion aerosol standard (Mini-CAST) soot generator, Aerosol Sci. Technol. 48 (2014) 467–479, https://doi.org/10.1080/02786826.2014.890694.

[36] K.S. Hong, K.S. Lee, S. Song, K.M. Chun, D. Chung, S. Min, Parametric study on particle size and SOF effects on EGR cooler fouling, Atmos. Environ. 45 (2011) 5677–5683, https://doi.org/10.1016/j.atmosenv.2011.07.036.

[37] L. Durdina, P. Lobo, M.B. Trueblood, E.A. Black, S. Achterberg, D.E. Hagen, B. T. Brem, J. Wang, Response of real-time black carbon mass instruments to mini-CAST soot, Aerosol Sci. Technol. 50 (2016) 906–918, https://doi.org/10.1080/02786826.2016.1204423.

[38] M. Lapuerta, F.J. Martos, J.M. Herreros, Effect of engine operating conditions on the size of primary particles composing diesel soot agglomerates, J. Aerosol Sci. 38 (2007) 455–466, https://doi.org/10.1016/j.jaerosci.2007.02.001.

[39] Paz C., Suárez E., B. López, Gas and particle size characterizations of a soot generator for fouling studies in EGR systems, in: 12th International Conference on Heat Transfer, Fluid Mechanics and Thermodynamics, 2016.

[40] M. Lapuerta, F.J. Martos, J.J. Expósito, Morphological characterization of diesel soot agglomerates based on the Beer-Lambert law, Meas. Sci. Technol. 24 (2013), 035405, https://doi.org/10.1088/0957-0233/24/3/035405.

[41] R. Zhang, Y. Zhang, S. Kook, Comparison between in-flame and exhaust soot particles in a single-cylinder, light-duty diesel engine, 19th Australasian Fluid Mechanics Conference (2014).

[42] P. Arora, S. Jain, Morphological characteristics of particles emitted from combustion of different fuels in improved and traditional cookstoves, J. Aerosol Sci. 82 (2015) 13–23, https://doi.org/10.1016/j.jaerosci.2014.12.006.

[43] J. Lee, I. Altman, M. Choi, Design of thermophoretic probe for precise particle sampling, J. Aerosol Sci. 39 (2008) 418–431, https://doi.org/10.1016/j.jaerosci.2008.01.001.

[44] O. Orhan, E. Haffner-Staton, A.L. Rocca, M. Fay, Characterisation of flame-generated soot and soot-in-oil using electron tomography volume reconstructions and comparison with traditional 2D-TEM measurements, Tribol. Int. 104 (2016) 272–284, https://doi.org/10.1016/j.triboint.2016.09.015.

[45] A.I. Medalia, F.A. Heckman, Morphology of aggregates—II. Size and shape factors of carbon black aggregates from electron microscopy, Carbon 7 (1969) 567–582, https://doi.org/10.1016/0008-6223(69)90029-3.

[46] A. Neer, U. Koylu, Effect of operating conditions on the size, morphology, and concentration of submicrometer particulates emitted from a diesel engine,

Combust. Flame 146 (2006) 142–154, https://doi.org/10.1016/j.combustflame.2006.04.003.
[47] P. DeCarlo, J. Slowik, D. Worsnop, P. Davidovcits, J. Jimenez, Particle morphology and density characterization by combined mobility and aerodynamic diameter measurements. Part 1: theory, Aerosol Sci. Technol. 38 (2004), https://doi.org/10.1080/027868290903907.
[48] A. Smith, D. Peters, R. McPheat, S. Lukanihins, R. Grainger, Measuring black carbon spectral extinction in the visible and infrared, J. Geophys. 120 (2015) 9670–9683, https://doi.org/10.1002/2015JD023564.
[49] M. Lapuerta, R. Ballesteros, F.J. Martos, A method to determine the fractal dimension of diesel soot agglomerates, J. Colloid Interface Sci. 303 (2006) 149–158, https://doi.org/10.1016/j.jcis.2006.07.066.
[50] M. Lapuerta, F.J. Martos, G. Martín-González, Geometrical determination of the lacunarity of agglomerates with integer fractal dimension, J. Colloid Interface Sci. 346 (2010) 23–31, https://doi.org/10.1016/j.jcis.2010.02.016.
[51] M.R. Kholghy, Y. Afarin, A.D. Sediako, J. Barba, M. Lapuerta, C. Chu, J. Weingarten, B. Borshanpour, V. Chernov, M.J. Thomson, Comparison of multiple diagnostic techniques to study soot formation and morphology in a diffusion flame, Combust. Flame 176 (2017) 567–583, https://doi.org/10.1016/j.combustflame.2016.11.012.
[52] G.M. Wang, C.M. Sorensen, Diffusive mobility of fractal aggregates over the entire Knudsen number range, Phys. Rev. E 60 (1999), https://doi.org/10.1103/physreve.60.3036.
[53] C.M. Sorensen, The mobility of fractal aggregates: a review, Aerosol Sci. Technol. 45 (2011) 765–779, https://doi.org/10.1080/02786826.2011.560909.
[54] P. Kulkarni, P.A. Baron, C.M. Sorensen, M. Harper, Nonspherical Particle Measurement: Shape Factor, Fractals, and Fibers, in: P. Kulkarni, P.A. Baron, K. Willeke (Eds.), Aerosol Measurement, John Wiley & Sons, Ltd, 2011: pp. 507–547. 10.1002/9781118001684.ch23.
[55] A. Braun, F.E. Huggins, S. Seifert, J. Ilavsky, N. Shah, K.E. Kelly, A. Sarofim, G. P. Huffman, Size-range analysis of diesel soot with ultra-small angle X-ray scattering, Combust. Flame 137 (2004) 63–72, https://doi.org/10.1016/j.combustflame.2004.01.003.
[56] S. di Stasio, Observation of restructuring of nanoparticle soot aggregates in a diffusion flame by static light scattering, J. Aerosol Sci. 32 (2001) 509–524, https://doi.org/10.1016/S0021-8502(00)00098-7.
[57] P. Sjoholm, D.B. Ingham, M. Lehtimaki, L. Perttu-Roiha, H. Goodfellow, H. Torvela, Gas-cleaning technology, in: H. Goodfellow, E. Tähti (Eds.), Industrial Ventilation Design Guidebook, Academic Press, San Diego, 2001: pp. 1197–1316. 10.1016/B978-012289676-7/50016-3.
[58] H. Klingenberg, Automobile Exhaust Emission Testing, fourth ed., Springer, Berlin, 2000. 10.1007/978-3-642-80243-0.
[59] M.F. Chandler, Y. Teng, Ü.Ö. Köylü, Diesel engine particulate emissions: a comparison of mobility and microscopy size measurements, Proc. Combust. Inst. 31 (2007) 2971–2979, https://doi.org/10.1016/j.proci.2006.07.200.
[60] B. Hu, U. Koylu, Size and morphology of soot particulates sampled from a turbulent nonpremixed acetylene flame, Aerosol Sci. Technol. 38 (2004) 1009–1018, https://doi.org/10.1080/027868290519111.
[61] C.M. Megaridis, R.A. Dobbins, Morphological description of flame-generated materials, Combust. Sci. Technol. 71 (1990) 95–109, https://doi.org/10.1080/00102209008951626.
[62] C.M. Sorensen, J. Cai, N. Lu, Light-scattering measurements of monomer size, monomers per aggregate, and fractal dimension for soot aggregates in flames, Appl. Opt. 31 (1992) 6547–6557, https://doi.org/10.1364/AO.31.006547.
[63] L.A.A. Yahia, E. Gehin, B. Sagot, Application of the TheRmophoretic Annular Precipitator (TRAP) for the study of soot aggregates morphological influence on their thermophoretic behaviour, J. Aerosol Sci. 113 (2017) 40–51, https://doi.org/10.1016/j.jaerosci.2017.07.018.
[64] P.M. Anderson, H. Guo, P.B. Sunderland, Repeatability and reproducibility of TEM soot primary particle size measurements and comparison of automated methods, J. Aerosol Sci. 114 (2017) 317–326, https://doi.org/10.1016/j.jaerosci.2017.10.002.
[65] E. Brugière, F. Gensdarmes, F.X. Ouf, J. Yon, A. Coppalle, Increase in thermophoretic velocity of carbon aggregates as a function of particle size, J. Aerosol Sci. 76 (2014) 87–97, https://doi.org/10.1016/j.jaerosci.2014.06.007.
[66] S. Talukdar, X. Li, M. T. Swihart, Photothermal aerosol synthesis and characterization of silicon nanoparticles, in: M.T. Swihart, M.D. Allendorf, M. Meyyappan (Ed.), Fundamental Gas-Phase and Surface Chemistry of Vapor-Phase Deposition II, 2001: pp. 448-454.
[67] R.S. Gilmore, Single particle detection and measurement (1st ed.), CRC Press, 1992. 10.1201/9781003069430.
[68] M. Lapuerta, R. Ballesteros, F. Martos, The effect of diesel engine conditions on the size and morphology of soot particles, Int. J. Veh. Des. 50 (2009), https://doi.org/10.1504/IJVD.2009.024972.
[69] K. Park, D. Kittelson, P. McMurry, Structural properties of diesel exhaust particles measured by transmission electron microscopy (TEM): relationships to particle mass and mobility, Aerosol Sci. Technol. 38 (2004) 881–889, https://doi.org/10.1080/027868290505189.
[70] G. Skillas, S. Künzel, H. Burtscher, U. Baltensperger, K. Siegmann, High fractal-like dimension of diesel soot agglomerates, J. Aerosol Sci. 29 (1998) 411–419, https://doi.org/10.1016/S0021-8502(97)00448-5.
[71] K. Lee, J. Zhu, S. Ciatti, M. Choi, D. Univ, Sizes, graphitic structures and fractal geometry of light-duty diesel engine particulates, SAE Tech. Pap. (2003), https://doi.org/10.4271/2003-01-3169.
[72] C.M. Sorensen, W. Kim, D. Fry, D. Shi, A. Chakrabarti, Observation of soot superaggregates with a fractal dimension of 2.6 in laminar acetylene/air diffusion flames, Langmuir 19 (2003) 7560–7563, https://doi.org/10.1021/la034063h.
[73] H.M.F. Amin, W.L. Roberts, An experimental apparatus to measure soot morphology at high pressures using multi-angle light scattering, Meas. Sci. Technol. 30 (2019), 075902, https://doi.org/10.1088/1361-6501/ab1c3f.
[74] M. Abegglen, L. Durdina, B.T. Brem, J. Wang, T. Rindlisbacher, J.C. Corbin, U. Lohmann, B. Sierau, Effective density and mass–mobility exponents of particulate matter in aircraft turbine exhaust: Dependence on engine thrust and particle size, J. Aerosol Sci. 88 (2015) 135–147, https://doi.org/10.1016/j.jaerosci.2015.06.003.
[75] S.C. Kim, J. Wang, W.G. Shin, J.H. Scheckman, D.Y.H. Pui, Structural properties and filter loading characteristics of soot agglomerates, Aerosol Sci. Technol. 43 (2009) 1033–1041, https://doi.org/10.1080/02786820903131081.
[76] J. Yon, A. Bescond, F. Liu, On the radiative properties of soot aggregates part 1: Necking and overlapping, J Quant Spectrosc Radiat Transf. 162 (2015) 197–206, https://doi.org/10.1016/j.jqsrt.2015.03.027.